Niphateolide A: Isolation from the marine sponge *Niphates olemda* and determination of its absolute configuration by an ECD analysis

Hikaru Kato[a], Tatsuo Nehira[b], Koichi Matsuo[c], Tetsuro Kawabata[a], Yoshihiro Kobashigawa[d], Hiroshi Morioka[d], Fitje Losung[e], Remy E. P. Mangindaan[e], Nicole J. de Voogd[f], Hideyoshi Yokosawa[g], and Sachiko Tsukamoto[a,*]

[a] *Department of Natural Medicines, Graduate School of Pharmaceutical Sciences, Kumamoto University, 5-1 Oe-honmachi, Kumamoto 862-0973, Japan*

[b] *Graduate School of Integrated Arts and Sciences, Hiroshima University, 1-7-1 Kagamiyama, Higashi-hiroshima 739-8521, Japan*

[c] *Hiroshima Synchrotron Radiation Center, Hiroshima University, 2-313 Kagamiyama, Higashi-Hiroshima, 739-0046, Japan*

[d] *Department of Analytical and Biophysical Chemistry, Graduate School of Pharmaceutical Sciences, Kumamoto University, 5-1 Oe-honmachi, Kumamoto 862-0973, Japan*

[e] *Faculty of Fisheries and Marine Science, Sam Ratulangi University, Kampus Bahu, Manado 95115, Indonesia*

[f] *Naturalis Biodiversity Center, P.O. Box 9517, 2300 RA Leiden, The Netherlands*

[g] *School of Pharmacy, Aichi Gakuin University, 1-100 Kusumoto-cho, Chikusa-ku, Nagoya 464-8650, Japan*

* Correspondence author. Tel: +81-96-371-4380; fax: +81-96-371-4380; e-mail address: sachiko@kumamoto-u.ac.jp (S. Tsukamoto).

Abstract

A diterpene with a new skeleton, niphateolide A (**1**), was isolated from the marine sponge, *Niphates olemda*, as an inhibitor of the p53-Hdm2 interaction. Its structure was elucidated by NMR spectroscopy and its absolute configuration was established as 10*R*,11*R* by ECD at the vacuum-ultraviolet region with a theoretical calculation. Compound **1** was observed as an inseparable stereoisomeric mixture at C-17 and an ECD analysis was subsequently performed by adopting a virtual equilibrium between the simplified two forms, 10*R*,11*R*,17*R*- and 10*R*,11*R*,17*S*-**1a**, in which the calculated ECD spectra were correctively integrated with the theoretically-derived internal and free energies.

Keywords: Diterpene, Marine sponge, *Niphates olemda*, ECD analysis

1. Introduction

Human tumors frequently have genetic mutations in the tumor suppressor p53 pathway.[1] Therefore, the p53 pathway is a prime target for new drugs in the treatment of cancer. Mdm2/Hdm2 (human Mdm2) is a ubiquitin ligase (E3) for p53 in the ubiquitin-proteasome system, and targeting Mdm2/Hdm2 represents a promising way to reactivate p53. During our continuing search for inhibitors of the p53-Hdm2 interaction in the treatment of cancer from natural sources, we have isolated (*R*)-hexylitaconic acid[2] and siladenoserinol A[3] from the marine-derived fungus *Arthrinium* sp. and a tunicate of the family Didemnidae, respectively, as inhibitors of this interaction. We herein described the isolation and structural elucidation of a diterpene with a new skeleton, designated niphateolide A (**1**) (Fig. 1), from the Indonesian marine sponge, *Niphates olemda*, as an inhibitor of the p53-Hdm2 interaction.

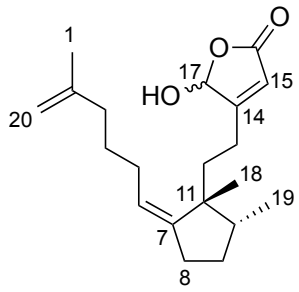

Fig. 1. Structure of niphateolide A (**1**).

2. Results

2.1. Isolation and structure elucidation of 1

Niphateolide A (**1**) was isolated from an EtOH extract of the marine sponge, *Niphates olemda*. The molecular formula of niphateolide A (**1**) was defined as $C_{20}H_{30}O_3$, based on an analysis of HRFABMS data (a deprotonated molecular ion peak at *m*/*z* 317.2121 [M - H]$^-$). The ^{1}H NMR

spectrum of **1** displayed four olefinic protons (δ 5.82 (s), 5.48 (br t), 4.69 (s), and 4.65 (s)), a downfield methine proton (δ 5.96 (s)), and three methyl protons (δ 1.70 (s), 1.07 (s), and 0.93 (d, *J* = 6.7 Hz)) (Table 1). The ^{13}C NMR spectrum (Table 1) showed characteristic 1:1 splitting signals for carbons, except for C-7, C-11, C-13, and C-14, which indicated that **1** was composed of a stereoisomeric mixture. An analysis of COSY spectroscopic data revealed the connectivity of three partial structures; substructures ***a*** (C-3/C-4/C-5/C-6), ***b*** (C-8/C-9/C-10/C-19), and ***c*** (C-12/C-13), as shown in Fig. 2. HMBC correlations from the terminal methylene H_2-20 (δ_H 4.65 (s) and 4.69 (s)) to C-1 (δ_C 22.43/22.45), C-2 (δ_C 145.95/145.96), and C-3 (δ_C 37.91/37.93) and from a methyl singlet H_3-1 (δ_H 1.70 (3H, s)) to C-2, C-3, and C-20 (δ_C 109.85/109.86) showed the presence of an isopropene group attached to substructure ***a***. The presence of a 2,3-dimethylcyclopentylidene moiety containing substructure ***b*** was established by HMBC correlations from a singlet methyl H_3-18 (δ_H 1.07 (s)) to C-7 (δ_C 141.8) and C-11 (δ_C 39.7) and from H_2-8 (δ_H 1.97 and 2.06) to C-7. HMBC correlations from H-6 (δ_H 5.48) to C-11 and from H_2-8 to C-6 (δ_C 122.17/122.25) suggested that the cyclopentylidene moiety was connected to substructure ***a***. HMBC correlations from H_2-12 (δ_H 4.55 and 1.69) to C-7 and from H_3-18 to C-12 (δ_C 32.52/32.55) indicated that substructure ***c*** was connected to C-11 of the cyclopentylidene moiety. The geometry of the double bond $\Delta^{6(7)}$ was determined to be *E* on the basis of the NOE correlations between H_2-5 and H_3-18 and between H-4 (δ 1.39) and H_2-13 (Fig. 3). The remaining formula $C_4H_3O_3$ contained low field carbons at δ_C 98.43/98.51, 117.12/117.17, 169.90/170.58, and 169.90. HMBC correlations from H-15 (δ_H 5.82) to C-13 (δ_C 24.0), C-14 (δ_C 169.90), C-16 (δ_C 169.90/170.58), and C-17 (δ_C 98.43/98.51), from H-17 (δ_H 5.96) to C-15 (δ_C 117.12/117.17) and C-16, and from H_2-13 (δ_H 2.29 and 2.39) to C-13, C-15, and C-17 showed the presence of a γ-hydroxybutenolide moiety attached to C-13 of substructure ***c*** (Fig. 2). Thus, the planar structure of **1** was established.

Table 1

NMR data[a] for **1** in $CDCl_3$

no.	δ_C[b]	δ_H (*J* in Hz)	HMBC[c]
1	22.43/22.45, CH_3	1.70, s	2, 3, 20
2	145.95/145.96, C		
3	37.91/37.93, CH_2	2.01, br t (7.3)	1, 2, 4, 5, 20
4	27.30/27.34, CH_2	1.39, m	6
		1.63, m	2, 6
5	30.73/30.75, CH_2	1.86, m	3, 4, 6, 7
		1.92, m	3, 4, 6, 7
6	122.17/122.25, CH	5.48, br t	4, 5, 11
7	141.8, C		
8	23.83/23.88, CH_2	1.97, m	6, 7
		2.06, m	6, 7
9	27.16/27.19, CH_2	1.54, m	
10	37.68/37.76, CH	1.60, m	18
11	39.7, C		
12	32.52/32.55, CH_2	1.55, m	7, 14, 18
		1.69, m	7, 14, 18
13	24.0, CH_2	2.29, m	12, 14, 15, 17
		2.39, m	12, 14, 15, 17
14	169.90, C		
15	117.12/117.17, CH	5.82, s	13, 14, 16, 17
16	169.90/170.58, C		
17	98.43/98.51, CH	5.96, s	15, 16
18	26.46/26.47, CH_3	1.07, s	7, 10, 11, 12
19	16.01/16.03, CH_3	0.93, d (6.7)	9, 10, 11
20	109.85/109.86, CH_2	4.65, s	1, 2, 3
		4.69, s	1, 2, 3

[a] ^1H NMR: 500 MHz, ^{13}C NMR: 125 MHz.

[b] Carbon signals, except for C7, C11, C13, and C14, appeared as 1:1 splitting.

[c] HMBC correlations were from proton(s) stated for the indicated carbon(s).

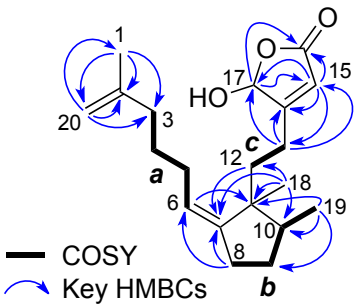

Fig. 2. COSY and key HMBCs observed in **1**.

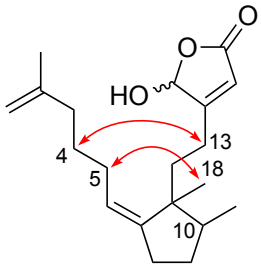

Fig. 3. Key NOE correlations (red arrows) observed in **1**.

Stereochemical interpretation was carried out for the two experimental observations, NOE correlations and ECD spectrum, with the help of computer simulations. In order to determine its relative configuration, all possible combinations, 10*R*,11*R*,17*R*- (a), 10*R*,11*R*,17*S*- (b), 10*S*,11*R*,17*R*- (c), and 10*S*,11*R*,17*S*-**1** (d), were subjected to a computer simulation (Fig. 4). Although C-10 and C-11 are included in a cyclopentane ring, the analysis with all the relevant conformations that occupied 99.9% of abundance for each isomer afforded the following result. Whereas the NOE correlation between H-10 and H_3-18 was accountable with their proximity in 10*R*,11*R*,17*R*- (a) and 10*R*,11*R*,17*S*-**1** (b) (2.43 and 2.34 Å, respectively), no corresponding proximity was observed in 10*S*,11*R*,17*R*- (c) or 10*S*,11*R*,17*S*-**1** (d) (3.72 and 3.71 Å, respectively), presumably due to steric hindrance between two methyl groups (H_3-18 and H_3-19) (Fig. 4). Moreover, no conformation of 10*S*,11*R*-isomer with >0.1% of abundance had H-10 and H_3-18 in

reasonable proximity for NOE correlation. These results indicated that the possibility of a 10*S**,11*R**-configuration was ruled out.

The absolute configuration was carefully elucidated by ECD experiment starting from the following two considerations. (1) In order to observe an interaction between the exocyclic double bond C-6/C-7 (185 nm)[4] and γ-hydroxybutenolide (207 nm),[5] which only exhibited a portion of one wing from the exciton-split CD in the regular ECD spectrum at 200 nm or longer, the spectrum was measured down to 180 nm in the vacuum-ultraviolet (VUV) region.[6-9] (2) In order to equilibrate epimerization at C-17, the both epimers of 10*R*,11*R*-**1a** (10*R*,11*R*,17*R*- and 10*R*,11*R*,17*S*-**1a**) were subjected to the ECD simulation. In our above-mentioned NOE analysis, the flexibility of the side chain with C-2/C-20 olefin was indicated. The divergence predicted in this conformational analysis was accordingly avoided with the simplified form **1a** (Fig. 5) by omitting the flexible side chain C-1/C-2/C-3/C-4, which was also based on the assumption that the contribution of an olefin in a flexible side chain to the whole shape of the ECD spectrum would be practically cancelled.[10,11] A standard calculation procedure[12] was carried out under these conditions, for the NOE-favorable epimers of 10*R*,11*R*-**1a** (10*R*,11*R*,17*R*- and 10*R*,11*R*,17*S*-**1a**). The conformer distribution was estimated from the Boltzmann's law giving 16 stable conformers that occupy 92.2% of abundance. Although all three theoretical ECD peaks at 189, 206, and 235 nm for 10*R*,11*R*,17*R*- and 10*R*,11*R*,17*S*-**1a** were opposite in sign to each other when analyzed separately (Fig. 6), a clear conclusion was derived by integrating all 10*R*,11*R*,17*R*- and 10*R*,11*R*,17*S*-**1a** conformers from the internal energies with free energy corrections (Fig. 6 and Tables S1).[13] Compared the simulated spectra with the experimental spectrum of **1**, 10*R*,11*R*-**1a** indicated good reproduction of ECD spectrum including the typical exciton-split CD corresponding to the absorption at 192 nm that is presumably from the interaction between the exocyclic double bond C-6/C-7 and γ-hydroxybutenolide (Fig. 6). The accuracy of the theoretical ECD spectra for each conformer was confirmed from the comparison of three frequently used functionals (B3LYP, CAM-B3LYP, and

BHandHLYP) that resulted in the same ECD sign patterns. Alternatively, ECD spectrum of the NOE-unfavorable pair 10*S*,11*R*-**1a** (10*S*,11*R*,17*R*- and 10*S*,11*R*,17*S*-**1a**) was also simulated in the same manner as of 10*R*,11*R*-**1a** (Table S3 and Fig. S7), resulting in poor reproduction of the experimental ECD spectrum with an extra split at 208 nm as well as a split at 192 nm. Therefore, the absolute configuration of **1** was determined to be 10*R*,11*R*.

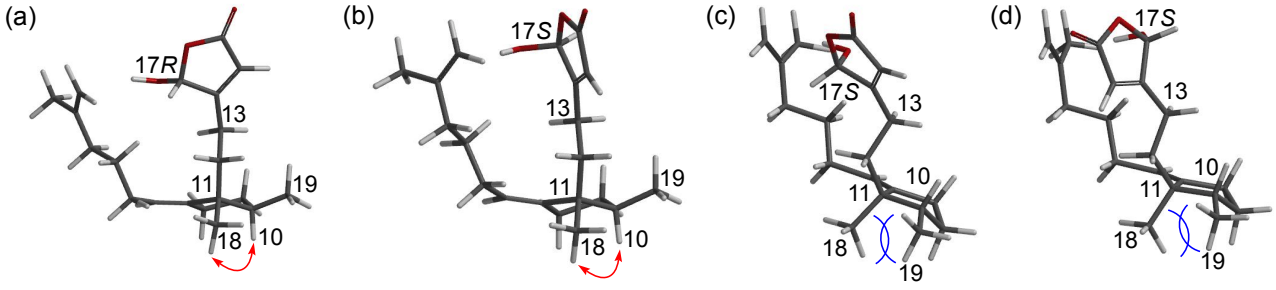

Fig. 4. Energy-minimized 10*R*,11*R*,17*R*- (a), 10*R*,11*R*,17*S*- (b), 10*S*,11*R*,17*R*- (c), and 10*S*,11*R*,17*S*-**1** (d) obtained from calculations with B3LYP/6-31G*. NOE correlations are shown in red arrows.

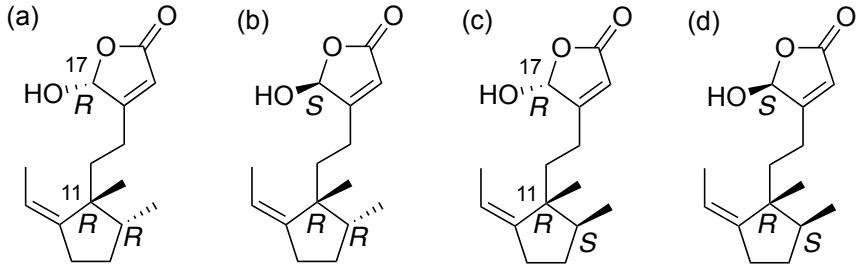

Fig. 5. Structures of four simplified forms, 10*R*,11*R*,17*R*- (a), 10*R*,11*R*,17*S*- (b), 10*S*,11*R*,17*R*- (c), and 10*S*,11*R*,17*S*-**1a** (d).

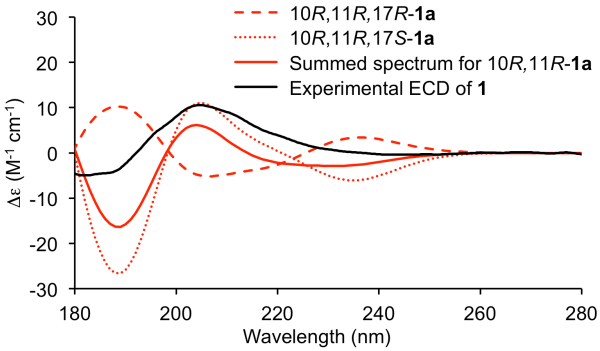

Fig. 6. Experimental VUV-ECD spectrum of **1** along with calculated ECD spectra of 10*R*,11*R*,17*R*- and 10*R*,11*R*,17*S*-**1a** and their summed spectrum based on internal energies with free energy corrections after optimization at the B3LYP/6-31G* level with the polarizable continuum model in CH_3CN.

2.3. Biosynthetic pathway of 1

Niphateolide A (**1**) may be biosynthetically derived from farnesyl pyrophosphate (FPP) via a 1,3-rearrangement of the methyl group from C-6 to C-11 (Scheme 1). Terpenoides containing a γ-hydroxybutenolide moiety were previously isolated from marine sponges and bear cyclohexane rings on the opposite terminals to the γ-hydroxybutenolide moieties.[14-16] In contrast, **1** had a cyclopentane ring in the middle of the side chain. This structural point of view allowed us to conclude that the carbon skeleton of **1** is new and therefore the structure of **1** was unique.

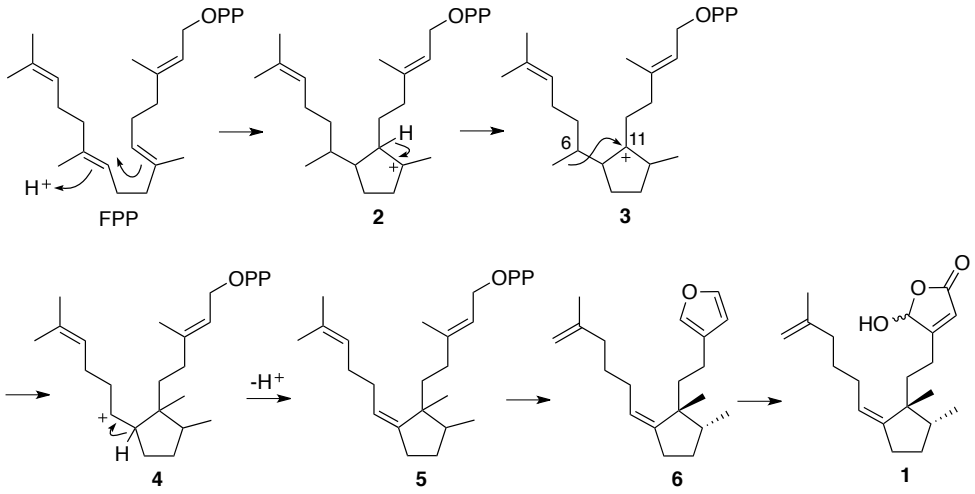

Scheme 1. Proposed biosynthetic pathway of **1**. FPP, farnesyl pyrophosphate.

2.4. Biological activity of 1

The inhibitory effect of **1** on the p53-Hdm2 interaction was examined using ELISA. Compound **1** inhibited the interaction with an IC_{50} value of 16 μM.

3. Experimental

3.1. General experimental procedure

Optical rotation was measured on a JASCO DIP-1000 polarimeter in MeOH. UV absorption was measured on a JASCO V-550 spectrophotometer in MeOH. Measurement of the VUV-ECD spectrum was performed with the spectrophotometer constructed at the Hiroshima Synchrotron Radiation Center. An IR spectrum was recorded on a PerkinElmer Frontier FT-IR spectrophotometer. NMR spectra were recorded on a Bruker Avance 500 NMR spectrometer in $CDCl_3$. Chemical shifts were referenced to the residual solvent peaks (δ_H 7.24 and δ_C 77.0). FABMS were measured on a JEOL JMS-700 MStation mass spectrometer.

3.2. Animal material. The marine sponge, *Niphates olemda*, was collected by scuba at a depth of 10 m in Mantehage, North Sulawesi, Indonesia, in December 2006 and immediately soaked in EtOH. A voucher specimen (RMNH POR 8526) of the sponge has been deposited in the Naturalis Biodiversity Center, the Netherlands.

3.3. Extraction and isolation. The marine sponge, *Niphates olemda* (100 g, wet weight), was extracted with EtOH. After evaporation, the residual aqueous solution was extracted with EtOAc. The EtOAc fraction (31 mg) was partitioned between *n*-hexane and 90% MeOH-H_2O. The 90% MeOH-H_2O fraction (10 mg) was purified by gel-filtration HPLC (Asahipak GS-310P column,

Asahi Chemical Industry Co., Ltd., 21.5 x 500 mm) with MeOH to afford niphateolide A (**1**) (1.2 mg).

3.4. Niphateolide A (1)

$[\alpha]^{20}_{D}$ +13° (*c* 0.46, MeOH); IR (film) ν_{max} 3291, 2930, 2756, 2738, 1648, 1456, 1265, 1126, 734 cm^{-1}; UV λ_{max} (MeOH) 204 nm (log ε 4.1); ^{1}H and ^{13}C NMR data, see Table 1; HRFABMS $[M–H]^-$ *m*/*z* 317.2121 (calcd for $C_{20}H_{29}O_3$, 317.2117).

3.5. ECD calculations for 10*R*,11*R*,17*R*-, 10*R*,11*R*,17*S*-, 10*S*,11*R*,17*R*-, and 10*S*,11*R*,17*S*-1a

Conformational searches were performed with CONFLEX7 (Ver. 7.A.0910 by CONFLEX, Tokyo)[17,18] using a commercially available PC (operating system: Windows 7 Professional SP1 64-bit, CPU: QuadCore Xeon E3-1225 processor 3.10 GHz, RAM 8 GB) and DFT calculations were conducted with Gaussian09 (Revivion A.02 by Gaussian, Wallingford, CT)[19] with a PC (Operating System: CentOS a Linux, CPU: 2 Intel Xeon 3 5550 processors 2.67 GHz, RAM 24 GB). The input structures of 10*R*,11*R*,17*R*- and 10*R*,11*R*,17*S*-**1a** were constructed on a graphical user interface considering the absolute configurations of interest, and were subjected to conformational searches with CONFLEX7 using MMFF94S (2010-12-04HG) as the force field, in which the initial stable conformers were generated for up to 50 kcal/mol. The given stable conformers of >1% population (14 and 13 conformers for 10*R*,11*R*,17*R*- and 10*R*,11*R*,17*S*-**1a**, respectively) were further optimized by the DFT method with B3LYP/6-31G*, supposing acetonitrile as the solvent with a polarizable continuum model (PCM). The dominant conformers obtained were chosen to cover >90% of the population from the Boltzmann's law at 298 K, for which their internal energies were analyzed with/without free energy corrections. Time-dependent density functional theory (TDDFT) calculations at the CAM-B3LYP/TZVP level with PCM

(acetonitrile) were performed for these conformers, leading to rotational strengths for 24 excited states. These rotational strengths were converted into Gaussian curves (bandwidth sigma = 3300 cm^{-1}) for the ECD spectrum of each conformer, in which no wavelength correction was employed because the corresponding electronic transitions led to the reproduction of the UV absorbance peak at 192 nm. These spectra were then correctively summed to give the resultant theoretical ECD spectrum of 10*R*,11*R*-**1a** (Fig. 6). As a comparison, TDDFT calculations were also performed with the other hybrid functionals B3LYP and BHandHLYP in the same manner as described above. ECD simulation of 10*S*,11*R*-**1a** (Fig. S7) was performed in the same procedure.

3.6. Conformational analyses of 10*R*,11*R*,17*R*-, 10*R*,11*R*,17*S*-, 10*S*,11*R*,17*R*-, and 10*S*,11*R*,17*S*-1

All calculations were performed with Spartan'14 (Ver. 1.1.8 by Wavefunction Inc., Irvine, CA) using a commercially available PC (operating system: Windows 7 Professional SP1 64-bit, CPU: QuadCore Core i7-3770 processor 3.40 GHz, RAM 8 GB). Stable conformers up to 10 kcal/mol for 10*R*,11*R*,17*R*-, 10*R*,11*R*,17*S*-, 10*S*,11*R*,17*R*-, and 10*S*,11*R*,17*S*-**1** were initially searched with MMFF.[20] All stable conformers were further optimized by the Hartree-Fock (HF) method with 3-21G. The resultant conformers of >0.1% were finally optimized by the density functional theory (DFT) method with B3LYP/6-31G*, giving stable conformers for each of the four relative configurations of interest. The proximity between H-10 and H_3-18 was thoroughly analyzed for all stable conformers obtained.

3.7. p53-Hdm2 interaction inhibition assay

Escherichia coli BL21 (DE3) cells transformed with pGEX6P1-p53 or pGEX6P1-HDM2 were precultured overnight at 37 °C in a 2xYT medium supplemented with 100 μg/mL ampicillin, transferred to a 40-fold volume of the same medium, and cultured at 37 °C. Isopropyl

1-thio-β-D-galactoside was then added at a final concentration of 0.1 mM when the optical density value at 600 nm reached 0.6, and cells were further cultured at 25 °C overnight. Cells were then harvested by centrifugation and suspended in PBS. The cells were disrupted by sonication, and the debris was removed by centrifugation. The supernatant was loaded onto glutathione-immobilized agarose beads (Nacalai Tesque) previously equilibrated with a buffer containing 50 mM Tris-HCl (pH 7.0), 150 mM NaCl, 0.1 mM dithiothreitol, 0.1 mM EDTA, and 0.01% Triton X-100, denoted by GST-buffer. These beads were washed three times with GST-buffer, and PreScission protease (GE Healthcare) was added to remove the GST tag from the GST-p53 or GST-Hdm2 protein. p53 or Hdm2 was then eluted from the beads with GST-buffer. Inhibition of the p53-Hdm2 interaction was tested by ELISA with a 96-well plate (F96 maxisorp immuno plate) (Nunc). Human p53 diluted in PBS was coated onto a 96-well plate and incubated at 4 ˚C overnight. The wells were extensively washed with 0.05% Tween 20 in PBS (PBST) and incubated with 5% bovine serum albumin (BSA) (Sigma) in PBS at 37 ˚C for 1.5 h. After washing with PBST, the wells were incubated for 1.5 h with a mixture of Hdm2 and a test sample diluted in PBS that had been previously incubated at 37 ˚C for 15 min. The wells were thoroughly washed with PBST and incubated with a primary anti-Hdm2 antibody (Santa Cruz, SMP14) in 5% BSA in PBST for 1.5 h, followed by a second antibody (mouse IgG-HRP) (GE Healthcare) in 5% BSA in PBST for 1.5 h. After washing with PBST and then citrate-phosphate buffer (pH 5.0), a mixture of *o*-phenylene diamine and 0.007% H_2O_2 in citrate-phosphate buffer was added to the wells, which were incubated at 37 ˚C for 30 min. Finally, 2 M H_2SO_4 was added to the wells and optical density at 490 nm was measured on a microplate reader. The IC_{50} value, the concentration required for 50% inhibition of the p53-Hdm2 interaction, was calculated from the results of duplicate experiments.

Acknowledgments

We thank Dr. H. Kobayashi of the University of Tokyo and Dr. H. Rotinsulu of Universitas Pembangunan for collecting the sponges. This work was supported by Grants-in-Aid for Scientific Research (Nos. 18406002, 25293025, and 26305005 to S.T.) from the Ministry of Education, Culture, Sports, Science, and Technology (MEXT) of Japan.

Supplementary data

NMR spectra of **1**, data for conformational analyses of 10*R*,11*R*- and 10*S*,11*R*-**1a**. These materials can be found, in the online version at http://dx.doi.org/10.1016/j.tet.2015.XX.XXX.

References and notes

1. Brown, C. J.; Lain, S.; Verma, C. S.; Fersht, A. R.; Lane, D. P. *Nat. Rev. Cancer* **2009**, *9*, 862-873.
2. Tsukamoto, S.; Yoshida, T.; Hosono, H.; Ohta, T.; Yokosawa, H. *Bioorg. Med. Chem. Lett.* **2006**, *16*, 69-71.
3. Nakamura, Y.; Kato, H.; Nishikawa, T.; Iwasaki, N.; Suwa, Y.; Rotinsulu, H.; Losung, F.; Maarisit, W.; Mangindaan, R. E. P.; Morioka, H.; Yokosawa, H.; Tsukamoto, S. *Org. Lett.* **2013**, *15*, 322-325.
4. An empirical method for predicting the bathochromic effect of alkyl substitution (5 nm) and exocyclic double bond (5 nm) was applied to λ_{max} value for exocyclic double bond C-6/C-7: 165 + (3 x 5) + 5 = 185 nm.
5. Shao, Y.; Wang, M.-F.; Ho, C.-T.; Chin, C.-K.; Yang, S.-W.; Cordell, G. A.; Lotter, H.; Wagner, H. *Phytochemistry* **1998**, *49*, 609-612.
6. Matsuo, K.; Gekko, K. *Bull. Chem. Soc. Jpn.* **2013**, *86*, 675–689.

7. Measurement of the VUV-ECD spectrum also disclosed an absorption peak at 192 nm when UV absorbance was derived from the high-tension voltage (Fig. S8).
8. Matsuo, K.; Yonehara, R.; Gekko, K. *J. Biochem.* **2004**, *135*, 405-411.
9. Takekawa, H.; Tanaka, K.; Fukushi, E.; Matsuo, K.; Nehira, T.; Hashimoto, M. *J. Nat. Prod.* **2013**, *76*, 1047–1051.
10. Yasui, H.; Akino, T.; Yasuda, T.; Fukada, M.; Wakamura, S.; Ono, H. *Tetrahedron Lett.* **2007**, *48*, 2395-2400.
11. Mori, K. *Tetrahedron Lett.* **2007**, *48*, 5609-5611.
12. Bringmann, G.; Bruhn, T.; Maksimenka, K.; Hemberger, Y. *Eur. J. Org. Chem.* **2009**, *21*, 2717-2727.
13. The same conclusion was derived from the two different distribution patterns that were derived from either the internal energies alone (Table S2) or those with the free energy correction (Table S1 and Fig. 6).
14. Yu, S.; Deng, Z; Proksch, P.; Lin, W. *J. Nat. Prod.* **2006**, *69*, 1330-1334.
15. Roll, D. M.; Ireland, C. M.; Lu, H. S. M.; Clardy, J. *J. Org. Chem.* **1988**, *53*, 3276-3278.
16. Elkhayat, E.; Edrada, R.; Ebel, R.; Wray, V.; van Soest R.; Wiryowidagdo, S.; Mohamed, M. H.; Müller, W. E. G.; Proksch, P. *J. Nat. Prod.* **2004**, *67*, 1809-1817.
17. Goto, H.; Obata, N.; Nakayama, N.; Ohta, K. *CONFLEX 7*, **2012**, CONFLEX Corporation, Tokyo, Japan.
18. (a) Goto, H.; Osawa, E., *J. Am. Chem. Soc.* **1989**, *111*, 8950-8951. (b) Goto, H.; Osawa, E., *J. Chem. Soc., Perkin Trans. 2* **1993**, 187-198.
19. Frisch, M. J.; Trucks, G. W.; Schlegel, H. B.; Scuseria, G. E.; Robb, M. A.; Cheeseman, J. R.; Scalmani, G.; Barone, V.; Mennucci, B.; Petersson, G. A.; Nakatsuji, H.; Caricato, M.; Li, X.; Hratchian, H. P.; Izmaylov, A. F.; Bloino, J.; Zheng, G.; Sonnenberg, J. L.; Hada, M.; Ehara, M.; Toyota, K.; Fukuda, R.; Hasegawa, J.; Ishida, M.; Nakajima, T.; Honda, Y.; Kitao, O.;

Nakai, H.; Vreven, T.; Montgomery, Jr., J. A.; Peralta, J. E.; Ogliaro, F.; Bearpark, M.; Heyd, J. J.; Brothers, E.; Kudin, K. N.; Staroverov, V. N.; Kobayashi, R.; Normand, J.; Raghavachari, K.; Rendell, A.; Burant, J. C.; Iyengar, S. S.; Tomasi, J.; Cossi, M.; Rega, N.; Millam, J. M.; Klene, M.; Knox, J. E.; Cross, J. B.; Bakken, V.; Adamo, C.; Jaramillo, J.; Gomperts, R.; R. E. Stratmann, R. E.; Yazyev, O.; Austin, A. J.; Cammi, R.; Pomelli, C.; Ochterski, J. W.; Martin, R. L.; Morokuma, K.; Zakrzewski, V. G.; Voth, G. A.; Salvador, P.; Dannenberg, J. J.; Dapprich, S.; Daniels, A. D.; Farkas, O.; Foresman, J. B.; Ortiz, J. V.; Cioslowski, J.; Fox, D. J. *Gaussian 09*, *Revision A.02*, **2009**, Gaussian, Inc., Wallingford CT.

20. Halgren, T. A. *J. Comp. Chem*. **1996**, *17*, 490-641.